Electronic Journal of Structural Engineering

Original Article

Cite this: DOI:10.56748/ejse.26915

Received Date: 08 November 2025
Accepted Date: 08 May 2026

1443-9255
https://ejsei.com/ejse

Effect of Buckling-Restrained Brace Cross-Sectional Shape on the Seismic Behavior of Inverted-V Concentrically Braced Frames

Jianfei Wang [a*]

[a] Architects & Engineers Co., Ltd. of Southeast University, Nanjing, 210096, China
* Corresponding author: wjfseu990102@163.com

Abstract

Conventional Concentrically Braced Frames (CBFs) exhibit asymmetric hysteretic response under seismic loading due to brace buckling, limiting energy dissipation. Buckling-Restrained Braced Frames (BRBFs) overcome this through buckling-restrained braces (BRBs) that yield stably in both tension and compression. This study presents a comparative finite element investigation of six BRB cross-sectional geometries circular, rectangular, diamond, elliptic-large (Ell-L, aspect ratio 2:1), elliptic-small (Ell-S, aspect ratio 1.5:1), and octagonal within an inverted-V CBF configuration under ATC-24 cyclic loading. Results reveal that cross-sectional geometry significantly affects the numerical performance indices, with the two elliptical configurations exhibiting distinct and complementary characteristics: Ell-S achieved the highest ductility among all specimens (μ = 9.02, approximately 177.5% improvement over the bare frame), while Ell-L attained the maximum initial lateral stiffness (Ki = 6.250 kN/mm, 76.06% improvement). The rectangular BRB configuration provided the highest peak lateral load capacity (Pmax = 495.14 kN, 126.76% increase). These findings demonstrate that BRB cross-section selection can tailor frame behavior for specific performance objectives within the adopted numerical framework: Ell-S for maximum ductility, Ell-L for maximum initial lateral stiffness, and rectangular sections for maximum peak lateral load capacity.

Keywords

Concentric Braced Frame, Buckling-Restrained Brace, Cross-Sectional Shape, Ductility, Lateral Load Resistance

1. Introduction

The adoption of Buckling-Restrained Braced Frames (BRBFs) in lieu of conventional Concentrically Braced Frames (CBFs) for both new construction and seismic rehabilitation projects has increased substantially in recent years (Chou et al., 2016; Guerrero et al., 2016; Hoveidae et al., 2015). This trend is driven by the inherent limitation of conventional CBFs: the susceptibility of compression braces to buckling, which results in asymmetric hysteretic response and diminished energy dissipation capacity under seismic loading. Consequently, extensive research efforts worldwide have focused on enhancing CBF performance through innovative structural configurations and advanced response mechanisms. These developments include the utilization of composite action, controlled metallic yielding, and high-performance materials (Issa et al., 2024; Li et al., 2024; Shen, 2023).

Extensive experimental investigations have been conducted on bracing components featuring a ductile steel core encased within a restraining mechanism that prevents local and global buckling (Dursun et al., 2023; Ghadami et al., 2024; Kontoni et al., 2023). The Buckling-Restrained Brace (BRB) exhibits stable and symmetric hysteretic behavior, thereby transmitting reduced force demands to foundations and adjacent structural elements (Bai et al., 2016). Typically, by concentrating inelastic action within a shortened yielding core segment, BRB configurations achieve lateral stiffness comparable to or exceeding that of conventional tension-compression CBFs, despite higher axial stresses. The BRB configuration originated in Japan as a supplemental energy dissipation device and was subsequently adopted in North America as a primary seismic force-resisting element (Black et al., 2004). Foundational BRB testing was reported by Watanabe et al. (A. Watanabe et al., 1988; N. Watanabe et al., 2003), who demonstrated that the brace configuration exhibits excellent ductility and energy dissipation capacity, while also highlighting the critical importance of adequate stiffness in the restraining mechanism. Subsequent advancements have led to the development of all-steel BRBs (Judd et al., 2016; Tremblay et al., 2006; Zhao et al., 2012). Numerical studies indicate that BRBFs exhibit significantly enhanced energy absorption and ductility compared to conventional CBFs, as reflected in more favorable seismic response modification factors (Shete et al., 2022).

Recent advances in computational engineering have highlighted the growing importance of mathematical modeling, numerical simulation, and parametric analysis in solving complex engineering problems (Islam et al., 2023). Such approaches have been applied to energy-related planning systems (Zoryna et al., 2022), wave propagation in elastoplastic media (Donayev and Ergashov, 2024), and heat transfer analysis under steady-state and boundary conditions (Alimov and Qudaybergenov, 2023, 2024). Similar computational strategies have also been used in thermal-fluid flow problems (Bibi et al., 2026; Nazeer et al., 2025; Kausar et al., 2025), finite-element treatment of boundary-value problems (Ernazarov et al., 2025), and optimization of engineering energy systems (Moradi et al., 2025; Pradhan et al., 2025). Moreover, generalized numerical formulations have been extended to differential models with complex constraints (Atamurodov et al., 2025; Gunasekar et al., 2025). Although these studies are not directly focused on buckling-restrained braced frames, they reflect the broader trend toward physics-based computational frameworks and systematic parametric investigation, which also underpins the present finite element study on the influence of BRB cross-sectional geometry on the seismic performance of concentrically braced frames.

Recent studies have further demonstrated the ongoing development of buckling-restrained braced systems toward enhanced seismic resilience, self-centering capability, and residual deformation control. Azizi et al. (2025) proposed synchronized double-stage yield buckling-restrained braces to improve the seismic performance of steel frames. Azizi (2025) numerically evaluated the cyclic and seismic behavior of three-core buckling-resistant braces with partially re-centering properties. In addition, Azizi et al. (2025) investigated the seismic performance of double-stage yield buckling restrained braced frames under mainshock-aftershock sequences, while Azizi and Ahmadi (2025) examined the mitigation of residual deformations in steel braced frames through an innovative Y-shaped hybrid buckling restrained brace. Moreover, Azizi et al. (2024) numerically studied the efficiency of self-centering two-yield buckling restrained braces in low-rise steel frames. Collectively, these studies confirm the growing research emphasis on advanced BRB configurations with improved energy dissipation, recentering behavior, and post-earthquake structural performance. Guo et al. (2025) investigated the seismic performance of a novel self-centering BRB with shape memory alloy bars, demonstrating enhanced recentering capacity and energy dissipation through experimental testing and numerical analysis. Liu et al. (2025) developed an innovative all-steel BRB with replaceable energy dissipation segments, showing that modular construction can facilitate post-earthquake repair while maintaining stable hysteretic behavior. Wang and Chen (2025) examined the effect of core plate slenderness on the low-cycle fatigue life of BRBs, providing critical insights into damage evolution and failure prediction under repeated seismic loading. Rahnavard et al. (2024) conducted a comprehensive numerical study on the cyclic behavior of BRBs with different core configurations, highlighting the influence of core geometry on stiffness degradation and energy dissipation capacity. These recent contributions underscore the continued evolution of BRB technology

toward enhanced reparability, fatigue resistance, and performance optimization areas directly relevant to the present investigation of cross-sectional shape effects.

Furthermore, the truss-confined BRB (TC-BRB) has been proposed to provide building structures with enhanced stiffness, strength, and energy dissipation capacity; experimental tests have confirmed that this configuration demonstrates stable and repeatable hysteretic response (Azevedo et al., 2023). Additionally, eccentricity in braced frames particularly in V-type CBFs—alters stress and strain distributions; with increasing eccentricity, the frame behavior may approach that of a moment-resisting frame (Naghavi et al., 2019). These findings underscore that careful consideration of cross-sectional design is essential for optimizing seismic performance and deformation capacity in BRBs within braced frame systems. Yeom and Yoo (2018) performed finite element analyses to investigate the effect of gusset plate clearance distance on the seismic behavior of inverted V-braced frames. The inverted-V configuration effectively reduces lateral drift in steel structures, thereby enhancing both stability and rigidity (Mishra et al., 2023). An innovative development in this field is the Assembled Self-Centering Buckling-Restrained Brace (ASC-BRB), which provides adjustable post-yield stiffness—a practical mechanism for controlling structural response across varying seismic intensity levels (Zhang et al., 2023). Collectively, these studies demonstrate that the integration of advanced materials, innovative designs, and optimized configurations is essential for achieving optimal performance of BRB systems in seismic applications. Recent research has advanced finite element modeling of steel elements under cyclic loading conditions. Ghadami and Pourmoosavi (2024) established a validated numerical model for low-yield-point steel links with exact predictions of cyclic behavior in terms of stiffness and damage. Ghadami et al. (2024) investigated buckling behavior in thin-walled steel elements, emphasizing the significance of mesh size and sensitivity to initial imperfections for local buckling behavior. Beyond these mechanical considerations, each cross-sectional shape presents distinct practical advantages and limitations that make it suitable for specific engineering applications, as summarized in Table 1.

Table 1. Summary of the key engineering characteristics and typical application scenarios for each cross-sectional shape

Cross-Section	Strength	Ductility	Fabrication Cost	Application Scenario
Circular	High	Moderate	High	High-rise, offshore, variable loading directions
Rectangular	High	High	Low	Low/mid-rise, seismic retrofit, cost-sensitive projects
Diamond	Moderate	Very High	Moderate	Essential facilities, performance-based design
Elliptical	High	Very High	Moderate-High	Structures requiring maximum energy dissipation
Octagonal	Moderate	High	Moderate	Modular construction, standardized connections

Despite the clear practical importance of cross-sectional geometry, no systematic study has compared these shapes under identical conditions to provide engineers with quantitative guidance for shape selection. Prior research has typically focused on optimizing a single geometry (e.g., improving rectangular BRB performance) rather than comparing multiple shapes. Furthermore, existing design provisions (AISC 341-22, EN 1998-1) treat BRBs generically without differentiating cross-sectional shape effects, potentially leading to suboptimal design choices.

As a matter of fact, there is a significant variation in stiffness, loading capacity, and ductility of a structure throughout its cross-section in reference to BRBs, and this variation significantly influences seismic performance. In this work, six cross-sectional shapes of BRBs are investigated, namely circular, rectangular, diamond, elliptical with two aspect ratios, and octagonal. We also assess their impact on the seismic performance of CBFs. We perform detailed finite element simulations in ABAQUS to thoroughly investigate these parameters. Our main aim is to identify the cross-sectional shape of BRBs that produces the most favorable seismic performance in CBFs in order to enhance safety and reliability in seismic design.

This study addresses the identified research gap by investigating the effect of six distinct BRB cross-sectional shapes on the seismic performance of an inverted-V concentrically braced frame. The primary objectives are:

1. To quantify the influence of cross-sectional shape on frame ductility, initial stiffness, and critical load capacity through systematic finite element analysis
2. To evaluate energy dissipation characteristics and failure mechanisms associated with each cross-sectional geometry
3. To identify optimal cross-sectional shapes for different seismic performance objectives (maximum strength, maximum ductility, balanced performance)
4. To provide quantitative guidance for performance-based design optimization of BRBF systems

The scope is limited to ST-37 steel BRBs with constant cross-sectional area, identical frame geometry, and cyclic loading following the ATC-24 protocol. This controlled parametric approach ensures that observed performance differences are attributable solely to cross-sectional shape.

2. Methods

2.1 Design Basics of Buckling-Restrained Braced

For designing the BRB, low-yield-strength steel is used as the core of concentrically braced members, with Teflon coating applied to the core surface, along with a separator and steel pipe covering the bracing assembly.

The BRB configuration examined in this study comprises a steel core encased within an outer restraining sleeve. To derive the critical buckling load, the system is idealized as two parallel structural elements subjected to the same lateral deformation but with different load-sharing mechanisms. The following assumptions are made:

1. Deformation compatibility: The steel core and outer sleeve undergo identical lateral deflections at any point along their length (no separation between components)
2. Load transfer: Axial load P is carried entirely by the steel core; the outer sleeve provides only flexural restraint and carries no axial load
3. No friction: The interface between core and sleeve is frictionless (ensured by Teflon coating)
4. Small deformations: Euler-Bernoulli beam theory applies
5. Linear elastic behavior: Both components remain elastic until buckling

To assess the buckling of a Euler column, the critical buckling load is determined for the steel core supported along the minor axis, employing the method below (Maleki and Mohammadi, 2017):

$$P_{cr-core} = \frac{n^2\pi^2(EI)_{core}}{(KL)^2} \quad (1)$$

where EI is the flexural stiffness around the weak axis, n denotes the number of buckling modes, and KL is the core brace's effective length. Critical buckling load can be calculated by solving the buckling of one beam-column in an elastic foundation or under uniform transverse load. If $q(x)$ is the uniformly distributed transverse load on the brace member, and EI_{core} and EI_{mantle} denote the flexural rigidity of the steel core and the outer restraining tube, respectively, the governing equations are written as follows:

$$(EI)_{mantel}\frac{d^4y(x)}{dx^4} = q(x) \quad (2)$$

$$(EI)_{core}\frac{d^4y(x)}{dx^4} + P\frac{d^2y(x)}{dx^2} = 0 \quad (3)$$

$$-(EI)_{mantel}\frac{d^4y(x)}{dx^4} = 0 \quad (4)$$

$$\frac{d^4y(x)}{dx^4} + \frac{P}{(EI)_{core} + (EI)_{mantel}}\frac{d^2y(x)}{dx^2} = 0 \quad (5)$$

By substituting the compatibility and equilibrium relations into the governing differential equation, Eq. (5) can be treated as a homogeneous eigenvalue problem for the lateral displacement of the brace. Applying the Euler-column boundary conditions at the brace ends and enforcing the non-trivial solution condition led to the characteristic equation, from which the critical buckling load can be derived and expressed as Eq. (6):

$$P_{cr-core} = \frac{n^2\pi^2}{(KL)^2}[(EI)_{core} + (EI)_{mantel}] \quad (6)$$

Since the buckling capacity around the weak axis of the steel core is significantly lower than that of the surrounding steel pipe, flexural deformations about the weak axis are neglected. Therefore, the critical buckling load of the brace (comprising both steel core and cover) is governed by the critical load of the outer pipe:

$$P_{cr-DB} = \frac{n^2\pi^2(EI)_{tube}}{(KL)^2} \quad (7)$$

In a properly constructed ductile brace, the load required to yield the steel core is considerably lower than the load that causes overall buckling of the brace assembly, as determined by Eq. (7). Consequently, the brace core is expected to yield under both compressive and tensile stresses. Accordingly:

$$(P_y)_{core} = (\sigma_y A)_{core} < P_{cr-DB} \quad (8)$$

This ensures that the core yields inelastically under both tension and compression before global buckling can occur.

2.2 FE Simulation

The finite element method has been widely employed in various structural engineering applications due to its capability to accurately simulate complex geometries, material nonlinearities, boundary conditions, and load–deformation responses of different structural systems (Malekzadeh et al., 2025; Pashaki et al., 2018; Adewunmi et al. 2024). This research utilized ABAQUS software to model structural elements (beams, columns, and bracing components) composed of ST-37 steel, as depicted in Fig. 1. The boundary conditions adopted in the finite element model are shown in Fig. 2. The column bases were assumed to be fully fixed, with all translational and rotational degrees of freedom restrained. The study applied cyclic loading derived from the ATC-24 protocol (Fig. 3), using displacement-controlled loading with yield displacements at multiples of 0.333, 0.667, 1, 2, and 3, each repeated for three cycles, followed by four loading phases until failure (two cycles per phase). This comprehensive cyclic loading protocol enabled detailed assessment of structural response, performance, and failure mechanisms.

To ensure numerical accuracy and computational efficiency, the finite element models were discretized using S4R reduced-integration shell elements. This element type is specifically suited for thin-walled steel sections where the thickness-to-width ratio is small, as it accurately captures membrane and bending behavior while avoiding shear locking. For the BRB configurations examined in this study featuring hollow cross-sections with thin walls shell elements provide an optimal balance between accuracy and computational cost, particularly for parametric studies involving multiple geometries. Mesh convergence studies were conducted to determine the optimal element size, establishing that element sizes ranging from 2 mm to 50 mm provide reliable solutions while maintaining reasonable computational cost. This range ensures accurate representation of stress gradients, particularly in regions of high stress concentration such as brace connections and gusset plates.

For clear identification and systematic comparison, specimen designations reflect the cross-sectional geometry of the BRB system: 'Cir' denotes circular, 'Rec' rectangular, 'Dia' diamond, 'Ell-L' elliptic-large (higher aspect ratio), 'Ell-S' elliptic-small (lower aspect ratio), and 'Oct' octagonal configurations. This nomenclature facilitates direct correlation between cross-sectional shape and observed performance metrics.

The material behavior of ST-37 steel was characterized using an elastic modulus (E_s) of 203 GPa, Poisson's ratio (ν_s) of 0.28, yield strength (f_y) of 263 MPa, and ultimate tensile strength (f_u) of 379 MPa (Naghavi et al., 2019). These values correspond to standard material properties for structural steel and ensure consistency with practical applications. The elastoplastic response was modeled using a bilinear elastic-plastic constitutive law with kinematic hardening, which adequately captures the cyclic behavior including Bauschinger effect a critical consideration for accurate simulation of seismic loading response.

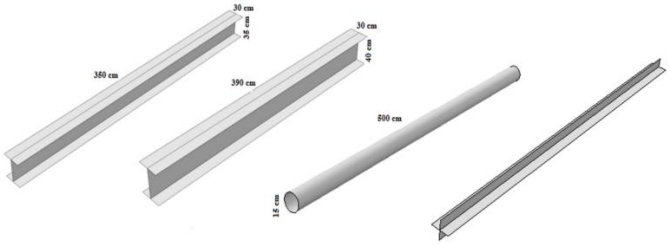

Fig. 1 Components of the model

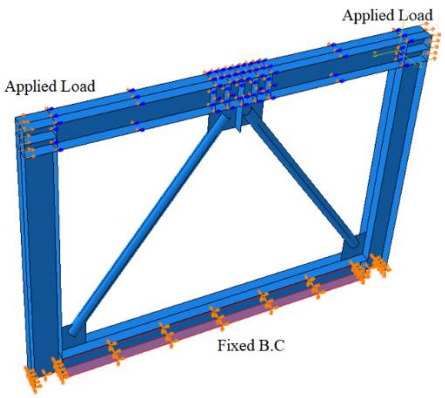

Fig. 2 Geometrical model and boundary condition of the models in ABAQUS

The study applied cyclic loading following the ATC-24 (1992) protocol for seismic testing of steel components (Fig. 3). This protocol uses displacement-controlled loading with amplitudes expressed as multiples of the yield displacement (δy), which is first determined from monotonic pushover analysis. For each specimen, the yield displacement δy was first established through nonlinear static pushover analysis, defined as the displacement at which significant yielding first occurs in the BRB core (identified by the point where the force-displacement curve deviates from linearity). For the CBF-Cir specimen, the characteristic displacement used for protocol normalization was determined from the monotonic pushover response through bilinear idealization of the base shear–lateral displacement curve. The physical significance of the multipliers is as follows:

- 0.333δy and 0.667δy: Sub-yield amplitudes used to characterize elastic stiffness and verify that no premature yielding occurs
- 1.0δy: The amplitude at which first yielding is expected, allowing verification of yield displacement prediction
- 2.0δy and 3.0δy: Ductility levels of 2 and 3, representing moderate inelastic demands typical of design-level earthquakes
- Subsequent amplitudes: Progressively increasing ductility demands up to failure, capturing ultimate capacity and degradation behavior

This protocol is widely used in seismic performance evaluation of steel structures because it systematically explores behavior from elastic through inelastic to failure, providing comprehensive data on stiffness degradation, energy dissipation, and failure mechanisms.

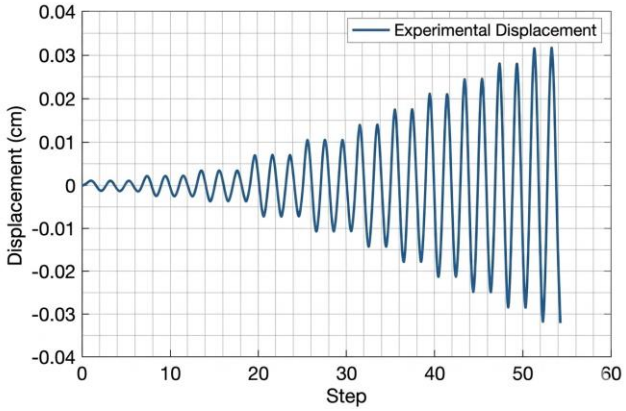

Fig. 3 ATC-24 cyclic loading protocol: Normalized displacement history showing amplitudes as multiples of yield displacement (δy). Cycles 1-3: 0.333δy; Cycles 4-6: 0.667δy; Cycles 7-9: 1.0δy; Cycles 10-12: 2.0δy; Cycles 13-15: 3.0δy; followed by increasing amplitudes to failure.

To accurately capture the cyclic response under seismic loading, a combined hardening model was implemented in ABAQUS, following the approach validated by Ghadami and Zare (2024) for steel components subjected to cyclic loading. The model incorporates both isotropic and kinematic hardening components to simulate the evolution of the yield surface under repeated inelastic cycles. For damage initiation and evolution, the ductile damage criterion available in ABAQUS was employed, with damage initiation defined by equivalent plastic strain at the onset of necking. Following the methodology recommended by Ghadami and Zare (2024), damage evolution was specified based on fracture energy to ensure mesh objectivity, using a characteristic element length and a linear damage evolution law. This approach captures strength degradation and eventual failure under cyclic loading, which is essential for accurate prediction of brace fracture and frame collapse mechanisms.

3. Results and Discussion

3.1 Mesh Sensitivity Analysis

A methodical mesh convergence study was carried out to ensure the accuracy and consistency of the numerical solution for all the geometrical configurations (Table 2). Five different mesh densities were used, corresponding to global mesh sizes of 2 mm, 5 mm, 10 mm, 25 mm, and 50 mm. The criteria for mesh convergence were based on three fundamental parameters, which are crucial for the assessment of seismic performance. These parameters are initial elastic stiffness, ultimate load capacity, and energy dissipation per cycle (Ghadami et al., 2024). Based on this convergence study, a global mesh size of 10 mm was selected for all production models, as further refinement to 5 mm produced changes of less than 2% in the monitored response quantities while increasing computational cost by approximately 130%. This 10 mm mesh provides an optimal balance between accuracy and computational efficiency for parametric study involving six cross-sectional geometries.

3.2 General Observations and Numerical Response

In this study, six BRBF specimens with different cross-sectional geometries are investigated. For each model, the characteristic yielding displacement was determined from the monotonic pushover response using a bilinear idealization of the base shear–lateral displacement curve. For example, Fig. 4 presents the force-deformation curve of the CBF-Cir specimen under monotonic loading. The results indicate that the CBF-Cir specimen reaches a peak lateral load of approximately 317 kN at a lateral displacement of about 141 mm. Subsequently, all specimens were analyzed under cyclic loading following the ATC-24 protocol. The initial lateral stiffness was calculated separately from the initial linear branch of the base shear–lateral displacement curve and should not be interpreted as the secant stiffness at the peak load.

Regarding initial geometric imperfections, a sensitivity study was conducted following the approach of Ghadami and Broujerdian (2018), who demonstrated that imperfection sensitivity in steel members varies with geometric properties. The first eigenmode was scaled to magnitudes of $L/1000$, $L/500$, and $L/200$ and introduced as initial imperfections. Results showed negligible variations (<2.1%) in ultimate load and energy dissipation compared to perfect geometry models. This imperfection insensitivity is attributed to the BRB restraining mechanism, which prevents buckling before core yielding (Eqs. 1–8). Accordingly, main parametric studies were conducted without explicit imperfection modeling.

Fig. 5 presents the von Mises stress distribution of the CBF-Cir specimen at a peak drift ratio of 2%. The maximum resultant stress was 256 MPa, which balanced the vertical component of the contact stress from the steel connection. The stress near the edges connected to the beam to the column is still high because of stress concentration. During the cyclic tests, all six specimens displayed stable deformations. Fig. 6 shows the force–displacement hysteresis response of the CBF-Cir specimen obtained from the cyclic analysis. The specimen clearly shows hysteretic behavior with a gradual transition from elastic to inelastic behavior at small displacements. The hysteresis response indicates that the specimen maintained its load-carrying capacity over most of the loading history, after which a gradual strength degradation occurred during the final five cycles preceding the last analysis step.

3.3 Hysteretic Behavior and Energy Dissipation

Figs. 7 and 8 present the cyclic load-displacement diagrams for the numerical models, compared to the base model lacking a steel brace. These cyclic diagrams are crucial for evaluating the seismic performance characteristics of lateral load-bearing systems, providing insight into parameters, namely, stiffness, energy dissipation, ductility, and resistance. The comparison of the diagrams shows that most of the increase in resistance can be attributed to the extreme points of the loading cycle. In particular, the peak lateral load of the base frame is 218.35 kN, whereas the CBF-Dia specimen reaches a peak lateral load of 296.23 kN, representing a 35.67% increase in load-carrying capacity compared with the base frame. The hysteresis loops exhibit noticeable pinching near the central region, which may be associated with localized inelastic deformation, stiffness degradation, and interaction effects in the bracing system. Nevertheless, the enlarged loop areas of the braced specimens compared with the bare frame indicate improved energy dissipation capacity. The reduced width in the central portion of the hysteresis loops may be associated with localized inelastic response and stiffness degradation in the bracing members during cyclic loading, thereby influencing the energy dissipation behavior of the frame. These hysteretic characteristics qualitatively suggest an improvement in the energy dissipation behavior of the braced configurations under cyclic loading. However, a quantitative comparison based on cumulative dissipated energy or hysteresis loop area is required to more rigorously substantiate this observation.

Table 2. The convergence study results for the CBF-Cir specimen

Mesh Size	Elements	Initial Stiffness (kN/mm)	Difference (%)	Ultimate Load (kN)	Difference (%)	Energy Dissipation (kJ)	Difference (%)
50 mm	1,248	5.477	-	308.2	-	112.4	-
25 mm	4,562	5.815	+6.2	316.7	+2.8	118.9	+5.8
10 mm	18,247	5.950	+2.3	317.8	+1.8	123.6	+4.0
5 mm	42,368	5.995	+0.8	320.1	+0.5	124.8	+1.0
2 mm	156,432	6.018	+0.4	321.8	+0.2	125.3	+0.4

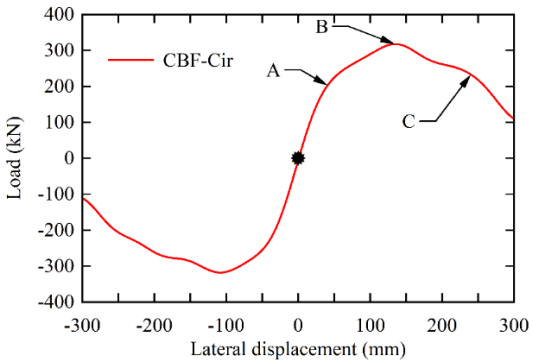

Fig. 4 The load–deformation curve of the CBF-Cir specimen

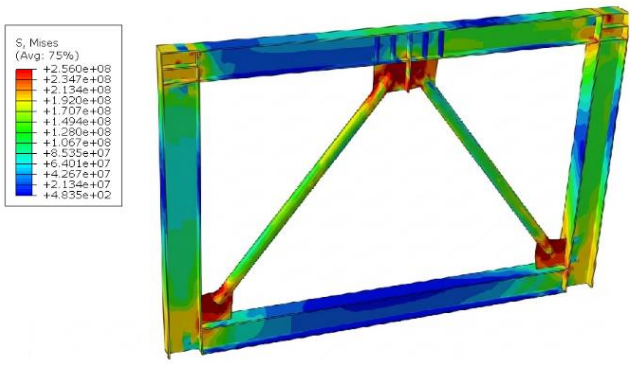

Fig. 5 von Mises stress (Pa) distribution in the CBF-Cir specimen at peak drift ratio of 2% (fully yielded state)

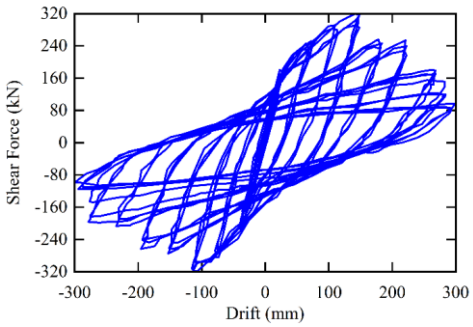

Fig. 6 Force–displacement hysteresis for the cyclic test of the CBF-Cir specimen

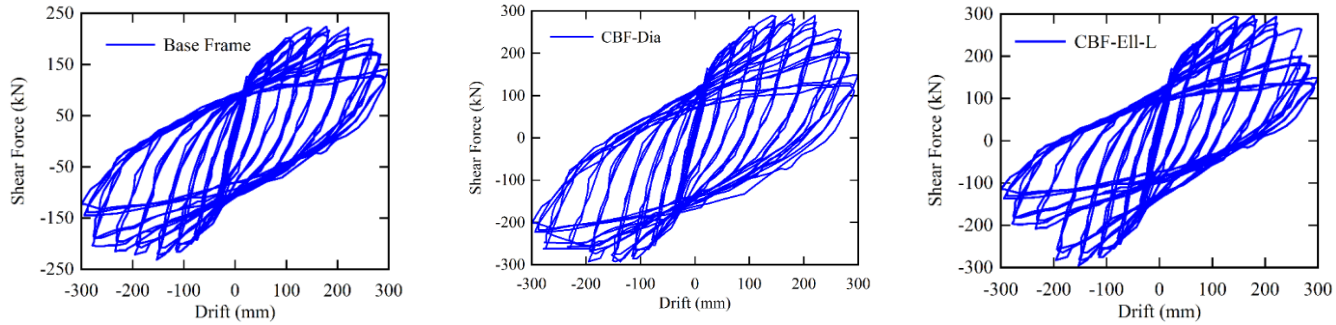

Fig. 7 Force–displacement hysteresis response of the base frame, CBF-Dia, and CBF-Ell-L specimens under cyclic loading

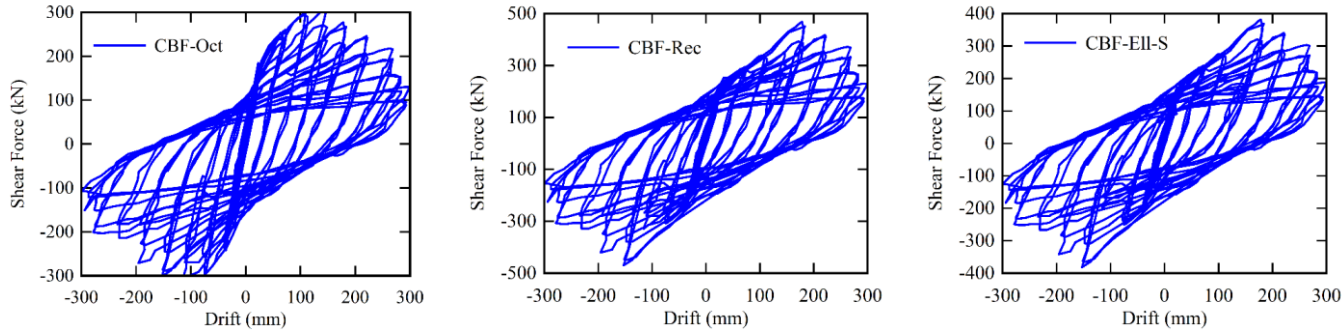

Fig. 8 Force–displacement hysteresis response of the CBF-Oct, CBF-Rec, and CBF-Ell-S specimens under cyclic loading

3.4 Stiffness, Strength, and Ductility Characteristics

Buckling-restrained braces in steel frames significantly enlarge the hysteresis-loop area, thereby enhancing the energy dissipation capacity and ductility of the frame. This leads to improved seismic resistance and reduced damage. Examination of the base shear–lateral displacement curves (Fig. 9) reveals that the peak lateral load capacity of the braced frame increased substantially compared with the bare frame. This enhancement is primarily attributed to the BRB members, particularly those arranged in the diagonal inverted-V configuration, which increases the load-bearing capacity and restrains out-of-plane instability. The numerical results show that the BRB-equipped frames exhibit improved load-carrying capacity and more stable cyclic response than the bare frame, indicating the beneficial effect of BRB incorporation on structural strength and ductility.

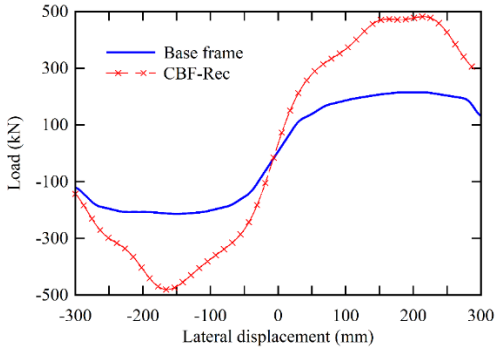

Fig. 9 Force–displacement pushover curves of the base frame and the CBF-Rec specimen

Figure 10 presents the force-displacement curves of enhanced finite element models alongside the base model for comparison. Performance improvements resulting from the modifications were derived from analysis of these curves. The enhanced models exhibit distinct force-displacement characteristics that highlight the advantages of the implemented design changes over the base model. These differences underscore the effects of the modifications on structural performance, including increased strength, ductility, and energy dissipation capacity. Comparative analysis demonstrates how these improvements contribute to a more robust and resilient structural response under loading conditions.

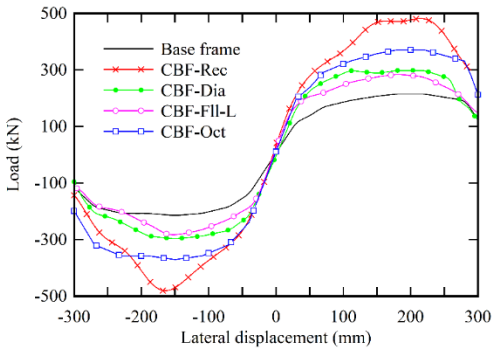

Fig. 10 Force-displacement pushover curves of base frame and bracing samples

3.5 Quantitative Comparison of Cross-Sectional Performance

Table 3 presents the ductility factors, initial stiffness values, and critical load capacities obtained from pushover analyses conducted on various braced steel frame specimens, using a base frame as the reference model. The equivalent ductility factor (μ) for each specimen was calculated using the following formula based on the force-displacement hysteresis curves obtained from cyclic analysis:

$$\mu=\Delta u/\Delta y \quad (9)$$

where Δu is the ultimate displacement corresponding to a 20% reduction in peak load capacity, and Δy is the yield displacement determined using the equivalent elastic-plastic energy method (Park, 1989). In this method, Δy is defined as the displacement at which the area under the actual force-displacement curve equals the area under an idealized bilinear elastic-perfectly plastic curve with the same initial stiffness and peak load. The initial lateral stiffness, K_i, was calculated from the slope of the initial linear branch of the base shear–lateral displacement curve:

$$K_i = \frac{\Delta V_b}{\Delta \delta} \quad (10)$$

where V_b is the base shear and δ is the lateral displacement of the frame. The stiffness values are reported in kN/mm and represent the global lateral stiffness of the frame, not the axial stiffness of an individual brace member. The peak lateral load, P_{max}, was obtained as the maximum lateral resistance reached in the pushover response.

Table 3. Equivalent ductility factor, initial lateral stiffness, and peak lateral load obtained from pushover curves of braced steel frames

Specimen	Aspect Ratio	Ductility	Initial lateral stiffness (kN/mm)	Peak lateral load (kN)	Improvement of peak lateral load (%)	Improvement of initial lateral stiffness (%)
Base frame	-	3.25	3.550	218.35	–	–
CBF-Cir	1:1	5.71	5.950	317.87	45.58	67.61
CBF-Dia	-	8.57	6.180	296.23	35.67	74.08
CBF-Ell-L	2:1	8.94	6.250	279.74	28.12	76.06
CBF-Ell-S	1.5:1	9.02	6.050	382.78	75.31	70.42
CBF-Rec	-	8.94	6.100	495.14	126.76	71.83
CBF-Oct	-	8.95	5.850	370.05	69.48	64.79

The base frame demonstrated a ductility factor of 3.25, an initial stiffness of 3.550 kN/mm, and a critical load of 218.35 kN. The enhanced models, incorporating different bracing configurations (CBF-Cir, CBF-Dia, CBF-Ell-L, CBF-Ell-S, CBF-Rec, and CBF-Oct), exhibited considerably higher values for ductility. The CBF-Ell-S specimen recorded the highest ductility factor at 9.02. The initial stiffness also varied among the specimens, with the CBF-Ell-L model achieving the maximum value of 6.250 kN/mm. Moreover, the CBF-Rec specimen can be considered the strongest configuration among the tested frames, as it exhibited the highest peak lateral load of 495.14 kN, which is substantially higher than that of the base frame. The results confirm that the tested brace configurations effectively improve the ductility and load-carrying capacity of steel frames. The enhanced ductility indicates that a greater portion of the input energy can be dissipated during loading. The increased initial stiffness and critical loads are a clear indication of the strengthened resistance to the applied forces. The enhanced models showed significant improvements, including ductility enhancements from 75.69% to 177.23%, initial stiffness increases from 64.79% to 76.06%, and critical load capacity enhancement up to 126.76% for the CBF-Rec specimen. These findings provide strong evidence for the effectiveness of the improved brace configurations in enhancing structural resilience and load-carrying capacity.

The major conclusion that can be drawn from this research is that elliptical BRBs are not a uniform entity; instead, they are a class of shapes whose properties are greatly dependent upon the aspect ratio. The two shapes studied are found to have significantly different properties. The Elliptic-Small (Ell-S) configuration, with an aspect ratio of 1.5:1, exhibited the highest ductility among all examined shapes, reaching a ductility factor of μ=9.02, corresponding to an approximately 177.54% enhancement over the bare frame. This behavior can be attributed to the more efficient distribution of material within the cross-section. The elliptical shape is able to grow a plastic zone that is able to enhance ductility significantly. However, the Elliptic-Large (Ell-L) configuration, with a 2:1 aspect ratio, attained the highest initial lateral stiffness of 6.250 kN/mm, corresponding to a 76.06% enhancement over the bare frame. The elongated elliptical geometry may increase the effective flexural contribution of the brace cross-section in the dominant deformation direction, thereby improving the initial lateral stiffness without increasing the cross-sectional area. The elliptical shapes are thus able to provide a lot of design flexibility by adjusting the aspect ratio to enhance ductility or stiffness as desired. The Ell-S is thus suitable for use in structures that are dependent upon energy dissipation, while the Ell-L is suitable for use in structures that are dependent upon initial stiffness.

4. Conclusion

This study investigated the effect of six BRB cross-sectional geometries circular, rectangular, diamond, elliptic-large (Ell-L, aspect ratio 2:1), elliptic-small (Ell-S, aspect ratio 1.5:1), and octagonal on the seismic performance of inverted-V concentrically braced frames under cyclic loading. The results showed that the selected cross-sectional geometry significantly influences the strength, stiffness, and ductility of the frame within the modeling framework adopted in this study.

Among the examined configurations, Ell-S exhibited the highest ductility (μ = 9.02, approximately 177.54% improvement), whereas Ell-L provided the maximum initial lateral stiffness (6.250 kN/mm, 76.06% improvement). The rectangular section achieved the highest peak lateral load capacity (495.14 kN, 126.76% increase) while maintaining high ductility, indicating its strong potential for strength-oriented design objectives. Diamond and octagonal sections also exhibited relatively balanced performance, combining substantial strength enhancement with high ductility. Within the modeling assumptions of the present study, these findings suggest that BRB cross-sectional shape can be used as an effective design parameter for tuning ductility, initial lateral stiffness, and peak lateral load capacity of BRB-equipped frames.

It should be noted, however, that the present conclusions are based on finite element simulations of a single inverted-V braced frame configuration subjected to a specific cyclic loading protocol. Moreover, the numerical results have not yet been validated against experimental data. Although S4R shell elements provide an efficient modeling strategy for thin-walled sections, they may not fully capture localized through-thickness stress and shear effects in critical regions. Therefore, future work should include experimental validation, investigation of additional frame configurations, and higher-fidelity numerical models to further verify the generality of the reported trends.

References

Adewunmi D, Samuel C, Fontana A (2024) Minimization of peeling stress in asymmetric single-lap adhesive joint via firefly optimization algorithm. Advances in Engineering and Intelligence Systems 3(2):18-34. https://doi.org/10.22034/aeis.2024.454482.1187

Alimov S, Qudaybergenov A (2023) Determination of temperature at the outer boundary of a body. Journal of Mathematical Sciences 274(2):159-171. https://doi.org/10.1007/s10958-023-06586-9

Alimov SA, Qudaybergenov AK (2024) Determining the steady-state temperature in an infinite layer. Differential Equations 60(8):1028-1041. https://doi.org/10.1134/S0012266124080044

Atamurodov S, Sayitqulov S, Toyirov A, Shikhnazarova G (2025) Approximate solutions for linear delay differential equations in medical applications. AIP Conference Proceedings 3356(1):020002. https://doi.org/10.1063/5.0296165

Azevedo IS, Silva ARD da, Silveira RAM da (2023) Influence of inverted-V-braced system on the stability and strength of multi-story steel frames. REM-International Engineering Journal 76(1):39-46. https://doi.org/10.1590/0370-44672022760017

Azizi H (2025) Numerical evaluation of cyclic and seismic performance of three-core buckling-resistant braces with partially re-centering properties. Structures 77:109078. https://doi.org/10.1016/j.istruc.2025.109078

Azizi H, Ahmadi J (2025) Mitigation of residual deformations in steel braced frames through an innovative Y-shaped hybrid buckling restrained braces. Journal of Constructional Steel Research 229:109533. https://doi.org/10.1016/j.jcsr.2025.109533

Azizi H, Ahmadi J, Kazemi F (2025) Enhancing seismic resilience in steel frames with synchronized double-stage yield buckling-restrained braces. Soil Dynamics and Earthquake Engineering 198:109587. https://doi.org/10.1016/j.soildyn.2025.109587

Azizi H, Ahmadi J, Nasserasadi K (2025) Seismic performance of double-stage yield buckling restrained braced frames under mainshock-aftershock sequences. Journal of Building Engineering 111:113141. https://doi.org/10.1016/j.jobe.2025.113141

Azizi H, Eghbali M, Ahmadi J (2024) Numerical investigation on the efficiency of self-centering two-yield buckling restrained brace on low-rise steel frames. International Journal of Civil Engineering 23(1):71-94. https://doi.org/10.1007/s40999-024-01032-6

Bai J, Ou J (2016) Earthquake-resistant design of buckling-restrained braced RC moment frames using performance-based plastic design method. Engineering Structures 107:66-79. https://doi.org/10.1016/j.engstruct.2015.10.048

Bibi B, Ali ABM, Ashraf M, Rasool G, Rashid MU, Sottarov A (2026) Transient mixed convection in coaxial pipes with temperature-dependent variable density. Dynamics of Atmospheres and Oceans 113:101649. https://doi.org/10.1016/j.dynatmoce.2026.101649

Black CJ, Makris N, Aiken ID (2004) Component testing, seismic evaluation and characterization of buckling-restrained braces. Journal of Structural Engineering 130(6):880-894. https://doi.org/10.1061/(ASCE)0733-9445(2004)130:6(880)

Chou C-C, Tsai W-J, Chung P-T (2016) Development and validation tests of a dual-core self-centering sandwiched buckling-restrained brace (SC-SBRB) for seismic resistance. Engineering Structures 121:30-41. https://doi.org/10.1016/j.engstruct.2016.04.015

Donayev B, Ergashov Y (2024) Investigation of the interaction of a plane wave with a moving massive barrier in a two-layer elastoplastic

medium. AIP Conference Proceedings 3119(1):020002. https://doi.org/10.1063/5.0215406

Dursun SE, Topkaya C (2023) Development of H-shaped hysteretic dampers for steel concentrically braced frames. Soil Dynamics and Earthquake Engineering 166:107758. https://doi.org/10.1016/j.soildyn.2023.107758

Ernazarov M, Mardonov E, Kulmirzayeva G, Mardonov B (2025) Solving the Sturm-Liouville boundary problem for a second-order ordinary differential equation by the finite element method. AIP Conference Proceedings 3377(1):020032. https://doi.org/10.1063/5.0299606

Ghadami A, Broujerdian V (2018) Shear behavior of steel plate girders considering variations in geometrical properties. Journal of Constructional Steel Research 153:567-577. https://doi.org/10.1016/j.jcsr.2018.11.009

Ghadami A, Ghamari A, Jaya RP (2024) Improving the behavior of the CBF system using an innovative box section damper: Experimental and numerical study. Structures 62:106210. https://doi.org/10.1016/j.istruc.2024.106210

Ghadami A, Jawdhari A, PourMoosavi G (2024) Buckling and post-buckling behavior of top flange coped I-beams with slender web panels. Thin-Walled Structures 203:111640. https://doi.org/10.1016/j.tws.2024.111640

Ghadami A, Pourmoosavi G (2024) An experimentally validated numerical model for generating the cyclic backbone curve of LYP links. Iran J Sci Technol Trans Civ Eng 48:4489-4504. https://doi.org/10.1007/s40996-024-01595-3

Ghadami A, Zare N (2024) Overstrength and rotation capacity of short and very short links made of ASTM A992 steel and subjected to AISC 341-22 loading protocol. Arabian Journal for Science and Engineering 50:1817-1831. https://doi.org/10.1007/s13369-024-09103-5

Guerrero H, Ji T, Teran-Gilmore A, Escobar JA (2016) A method for preliminary seismic design and assessment of low-rise structures protected with buckling-restrained braces. Engineering Structures 123:141-154. https://doi.org/10.1016/j.engstruct.2016.05.015

Gunasekar T, Nithyanandhan K, Hanumagowda BN, Tawade JV, Othman NA, Abdullaeva B, Batool N, Kurbonov K (2025) A study on intuitionistic fuzzy neutral functional integro-differential PDEs with impulses. Partial Differential Equations in Applied Mathematics 11:101296. https://doi.org/10.1016/j.padiff.2025.101296

Hoveidae N, Tremblay R, Rafezy B, Davaran A (2015) Numerical investigation of seismic behavior of short-core all-steel buckling restrained braces. Journal of Constructional Steel Research 114:89-99. https://doi.org/10.1016/j.jcsr.2015.06.005

Islam R, Sohel A, Bin Ashab MF (2023) Numerical investigation of motive pressure on condensation and evaporation process in steam ejector of renewable refrigeration system. Advances in Engineering and Intelligence Systems 2(4):11-22. https://doi.org/10.22034/aeis.2023.412043.1124

Issa A, Stephen S, Mwafy A (2024) Unveiling the seismic performance of concentrically braced steel frames: A comprehensive review. Sustainability 16(1):427. https://doi.org/10.3390/su16010427

Judd JP, Marinovic I, Eatherton MR, Hyder C, Phillips AR, Tola AT, Charney FA (2016) Cyclic tests of all-steel web-restrained buckling-restrained brace subassemblages. Journal of Constructional Steel Research 125:164-172. https://doi.org/10.1016/j.jcsr.2016.06.007

Kausar MS, Ali ABM, Anwar T, Sottarov A, Walelign T, Waqas M (2025) A computational framework for micropolar fluid considering chemical reaction in porous media with stagnation point flow over a stretchable sheet in the presence of viscous dissipation. International Journal of Thermofluids 30:101453. https://doi.org/10.1016/j.ijft.2025.101453

Kontoni DN, Ghamari A, Kheiri J, Ilia G (2023) An innovative I-shaped low-yield steel shear damper directly connected to the concentrically braced frame. Ce/Papers 6(3-4):925-929. https://doi.org/10.1002/cepa.2604

Li H, Zhang W (2024) Seismic energy and axial column demands of steel concentrically braced frames. Structures 64:106586. https://doi.org/10.1016/j.istruc.2024.106586

Maleki VA, Mohammadi N (2017) Buckling analysis of cracked functionally graded material column with piezoelectric patches. Smart Materials and Structures 26(3):035031. https://doi.org/10.1088/1361-665X/aa5324

Malekzadeh M, Shishesaz M, Mosalmani R, Arab Maleki V, Yaghootian A (2025) Carbon nanotube reinforced 3D printed PMMA filaments: Mechanical enhancement through experimental and multi-scale modeling. Materials Chemistry and Physics 345:131194. https://doi.org/10.1016/j.matchemphys.2025.131194

Mishra P, Vyavahare AY (2023) A critical review on buckling restrained braces. Građevinar 75(12):1165-1181. https://doi.org/10.14256/JCE.3778.2023

Moradi AM, Sadri F, Sassani M, Akhmadaliyeva N, Xudaynazarov E, Matchanova B, Masharipova G, Yuldashev F, Nurmatovich HA, Akhmedov U, Mamayusupova D, Sherov A, Yuldoshev J, Makhkamova D (2025) Modeling two-level interval and multi-objectives approach for energy optimization in the smart electrical grid with uncertainty of power prices and demand side management strategies. Results in Engineering 28:108384. https://doi.org/10.1016/j.rineng.2025.108384

Naghavi M, Rahnavard R, Thomas RJ, Malekinejad M (2019) Numerical evaluation of the hysteretic behavior of concentrically braced frames and buckling restrained brace frame systems. Journal of Building Engineering 22:415-428. https://doi.org/10.1016/j.jobe.2018.12.023

Nazeer M, Ali ABM, Hussain F, Beemkumar N, Kurbonov K, Jain V, Khan MI, Ben Khedher N (2025) Poiseuille flow of Jeffrey fluid with variable transport properties in porous media under magnetic and radiative effects. Dynamics of Atmospheres and Oceans 112:101599. https://doi.org/10.1016/j.dynatmoce.2025.101599

Park R (1989) Evaluation of ductility of structures and structural assemblages from laboratory testing. Bulletin of the New Zealand National Society for Earthquake Engineering 22(3):155-166. https://doi.org/10.5459/bnzsee.22.3.155-166

Pradhan R, Hajiyev E, Shichiyakh R, Kurikov V, Yuldoshev JE (2025) Optimal techno-economic feasibility of an off-grid microgrid system using load flow energy management strategies. Operations Research Forum 6:120. https://doi.org/10.1007/s43069-025-00524-y

Shen J (2023) Impact of unique practice in concentrically braced frames on their seismic performance. Journal of Constructional Steel Research 201:107718. https://doi.org/10.1016/j.jcsr.2022.107718

Shete PS, Madhekar SN, Ghowsi AF (2022) Finite element parametric studies on buckling restrained brace. ASPS Conference Proceedings 1(3):645-651. https://doi.org/10.38208/acp.v1.565

Tremblay R, Bolduc P, Neville R, DeVall R (2006) Seismic testing and performance of buckling-restrained bracing systems. Canadian Journal of Civil Engineering 33(2):183-198. https://doi.org/10.1139/l05-103

Vahidi Pashaki P, Pouya M, Maleki VA (2018) High-speed cryogenic machining of the carbon nanotube reinforced nanocomposites: Finite element analysis and simulation. Proceedings of the Institution of Mechanical Engineers, Part C: Journal of Mechanical Engineering Science 232(11):1927-1936. https://doi.org/10.1177/0954406217714012

Watanabe A, Hitomi Y, Saeki E, Wada A, Fujimoto M (1988) Properties of brace encased in buckling-restraining concrete and steel tube. Proceedings of Ninth World Conference on Earthquake Engineering 4:719-724.

Watanabe N, Kato M, Usami T, Kasai A (2003) Experimental study on cyclic elasto-plastic behavior of buckling-restraining braces. Journal of Earthquake Engineering 133.

Yeom H-J, Yoo J-H (2018) Analytical investigation on seismic behavior of inverted V-braced frames. International Journal of Steel Structures 18:189-198. https://doi.org/10.1007/s13296-018-0315-4

Zhang C, Zong S, Sui Z, Guo X (2023) Seismic performance of steel braced frames with innovative assembled self-centering buckling restrained braces with variable post-yield stiffness. Journal of Building Engineering 64:105667. https://doi.org/10.1016/j.jobe.2022.105667

Zhao J, Wu B, Ou J (2012) Effect of brace end rotation on the global buckling behavior of pin-connected buckling-restrained braces with end collars. Engineering Structures 40:240-253. https://doi.org/10.1016/j.engstruct.2012.02.030

Zoryna TG, Aliaksandrovich SA, Valeeva YS, Kalinina MV, Ilikova LE, Suvonovich EY (2022) Measures to stimulate the development of electric transport as a tool for the development of the territory. 2022 8th International Conference on Energy Efficiency and Agricultural Engineering (EE&AE). https://doi.org/10.1109/EEAE53789.2022.9831360

Disclaimer